

New Model of Cystic Fibrosis Transmembrane Conductance Regulator Proposes Active Channel-like Conformation

James Dalton,^{†,‡} Ori Kalid,^{‡,§} Maya Schushan,[‡] Nir Ben-Tal,^{*,‡} and Jordi Villà-Freixa^{*,†,§}

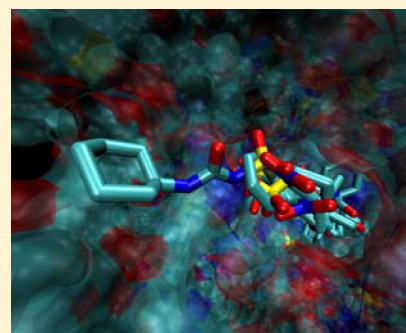
[†]Computational Biochemistry and Biophysics Laboratory, Research Unit on Biomedical Informatics, IMIM Hospital del Mar and Universitat Pompeu Fabra, C/Doctor Aiguader, 88, 08003 Barcelona, Catalunya, Spain

[‡]Department of Biochemistry and Molecular Biology, George S. Wise Faculty of Life Sciences, Tel-Aviv University, Ramat Aviv 69978, Israel

[§]Escola Politècnica Superior, Universitat de Vic, C/de la Laura 13, 08500 Vic, Catalunya, Spain

S Supporting Information

ABSTRACT: The cystic fibrosis transmembrane conductance regulator (CFTR) is an unusual ABC transporter, functioning as a chloride channel critical for fluid homeostasis in multiple organs. Disruption of CFTR function is associated with cystic fibrosis making it an attractive therapeutic target. In addition, CFTR blockers are being developed as potential antidiarrheals. CFTR drug discovery is hampered by the lack of high resolution structural data, and considerable efforts have been invested in modeling the channel structure. Although previously published CFTR models that have been made publicly available mostly agree with experimental data relating to the overall structure, they present the channel in an outward-facing conformation that does not agree with expected properties of a “channel-like” structure. Here, we make available a model of CFTR in such a “channel-like” conformation, derived by a unique modeling approach combining restrained homology modeling and ROSETTA refinement. In contrast to others, the present model is in agreement with expected channel properties such as pore shape, dimensions, solvent accessibility, and experimentally derived distances. We have used the model to explore the interaction of open channel blockers within the pore, revealing a common binding mode and ionic interaction with K95, in agreement with experimental data. The binding-site was further validated using a virtual screening enrichment experiment, suggesting the model might be suitable for drug discovery. In addition, we subjected the model to a molecular dynamics simulation, revealing previously unaddressed salt-bridge interactions that may be important for structure stability and pore-lining residues that may take part in Cl⁻ conductance.



■ INTRODUCTION

The cystic fibrosis transmembrane conductance regulator (CFTR) lies at the basis of the disorder cystic fibrosis (CF) and also conditions such as acute watery diarrhea (AWD). CF is the most common lethal disease among European descendants that is caused by a single-gene mutation,¹ and AWD becomes a major public health concern when access to clean water supply is scarce such as in natural disasters.² Infectious-based AWD is also the second most common cause of infant mortality worldwide.³ The CFTR gene was first identified in 1989, in region q31.2 on the long arm of human chromosome 7. The gene contains 27 exons encoding a protein of 1480 amino acids: a chloride efflux channel mostly found in the lumen-exposed surface of epithelial cells.⁴ Deletion of CFTR protein content or a decrease in its activity in epithelial cells of CF patients causes hyperabsorption of sodium chloride and a reduction in the periciliary salt and water content, thus impairing mucociliary clearance.⁵ To date, over 1900 mutations in the CFTR gene have been identified with the most common being a deletion of a single amino-acid, F508, which is found in at least one allele of ~90% of CF patients.⁶

Structurally, CFTR is a member of the human subfamily C of the ATP-Binding Cassette (ABC) transporter family, unique in being the only family member known to function as an ion channel.⁷ CFTR topology is similar to that of other ABC transporters (Figure 1), comprising two membrane spanning domains (MSDs), each linked through intracellular loops (ICLs) to a nucleotide binding domain (NBD). MSD1 contains transmembrane helices (TM) 1–6 and MSD2 contains TMs 7–12. Uniquely to CFTR, NBD1 and MSD2 are connected by a partially unstructured regulatory domain (R-region), which must be phosphorylated to enable channel gating.⁸ The F508del mutation in the first NBD almost completely abolishes correct cellular processing of CFTR in CF patients, probably by disrupting interdomain contacts required for the stability and correct folding of the multidomain protein,^{9–11} as well as destabilizing NBD1 itself.^{12,13} Most of the F508del mutant protein is targeted for endoplasmic reticulum-associated degradation (ERAD), and the few channels that make it to the plasma membrane are

Received: December 10, 2011

Published: July 2, 2012

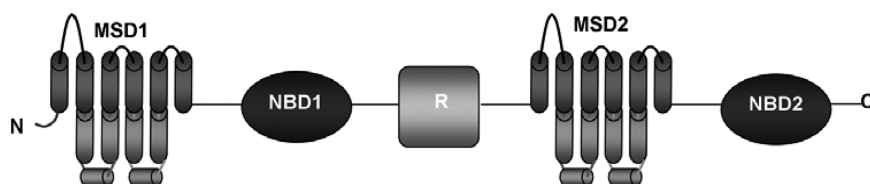


Figure 1. Domain arrangement of CFTR.

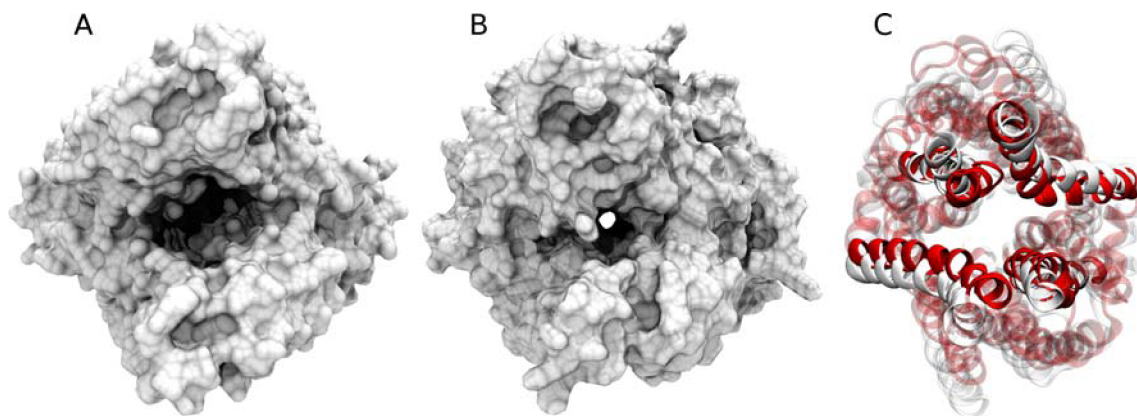


Figure 2. Outward-facing conformation of Sav1866 compared against the more compact channel-like conformation of a representative CFTR model, as viewed from the outer membrane side, visualized with visual molecular dynamics (VMD).³² (A) Molecular surface of Sav1866 outward-facing structure (2HYD). (B) Molecular surface of one of the ROSETTA models that passed validation, showing a more defined, compact, and continuous pore. (C) Cartoon representation of a transmembrane-region superposition of the same ROSETTA CFTR model (in red) and Sav1866 (in gray). The four central helices of CFTR: TM6, TM1, TM12, and TM7 (anticlockwise from top-left, respectively, and in opaque red) are observed to move inward, compared to the corresponding helices of Sav1866 (in opaque gray).

characterized by a reduced open probability and thermal instability, being rapidly endocytosed and targeted for lysosomal degradation.¹⁴

CFTR is an important component in AWD because the channel can become overstimulated, e.g. by cholera toxin, resulting in exaggerated ion transport and rapid water loss.² Currently there is no fast, effective treatment for AWD, with conventional rehydration therapies still being the best option.² Therefore, the discovery of a viable drug that specifically targets and inhibits CFTR could mean a new and efficient treatment for AWD. Efforts to develop a potent and bioavailable CFTR inhibitor recently culminated in the initiation of phase-I clinical trials with the iOWH032 by OneWorld Health.² Several chemical series of CFTR inhibitors have been discovered so far by high throughput screening, including thiazolidinones, glycine hydrazides, and pyrimido-pyrrolo-quinoxalinediones.^{15–18} These operate via distinct interaction modes with CFTR: thiazolidinones and pyrimido-pyrrolo-quinoxalinediones blocking from the intracellular side and glycine hydrazides operating at the extracellular side.^{18,19} In the absence of a high resolution structure of CFTR, structural models could facilitate further understanding of inhibitor interaction modes as well as discovery of novel channel blockers.

Several homology models of CFTR have previously been published, some of which have had their coordinates publicly released, e.g. refs 20–22, while others have not, e.g., refs 23 and 24. To our knowledge all of these models have been based on the crystal structure of the Sav1866 bacterial transporter,²⁵ except for one.²² This exception was modeled based upon the low-resolution closed apo-structure of the MsbA transporter, and, as such, modeled CFTR in a “closed” inactive state. As a consequence, it is not relevant here in terms of reaching a

channel-like structure of “active” CFTR. In addition, due to the nature of the template utilized, it may suffer from low accuracy. While the models based on Sav1866 are in agreement with a large body of experimental data, demonstrating that Sav1866 is an adequate homology modeling template for CFTR, the majority of these present CFTR in the Sav1866 “outward-facing” conformation.²⁵ This corresponds to a wide barrel-shaped channel structure which lacks the previously proposed architecture comprising outer and inner vestibules separated by a narrow region containing the chloride-specific selectivity filter^{23,24,26–28} (Supporting Information (SI) Figure S1). One exception to this may be a model that was published while our manuscript was being reviewed.²⁴ This model is a modified version of one previously published²³ and may possibly be the first that displays an approximately correct CFTR architecture, including a narrow pore region. However, as the coordinates of this newly published model have not been publicly released, a detailed examination of its architecture is not possible. A potential limitation of this recent model is a premature termination of the conduction path at the cytoplasmic end with no apparent point of entry, which the authors attribute to the properties of the Sav1866 structural template.²⁴ In addition, the authors report that some of the MD conformations are too constricted to allow for chloride ion passage through the selectivity filter region.²⁴

Our objective in this study was to provide an improved representation of the ion conducting conformation of CFTR, by deriving a “channel-like” conformation from the Sav1866 outward-facing structure, possessing a continuous pore as well as complete inner and outer vestibules separated by a physically plausible narrow region corresponding to the proposed selectivity filter.^{23,24,26–28} This was accomplished by using a unique modeling protocol incorporating pore chloride ions and

guided by an extensive set of experimentally derived constraints based on pore dimensions, salt-bridges, inter-residue cross-linking distances, and residue accessibility. The motivation for this project was twofold: first, such a model could provide further structural insight into the function of CFTR and its malfunction in CF; and second, it could conceivably provide an improved structure-based framework for the design of CFTR channel blockers as potential anti-diarrheals,²⁹ as well as CFTR modulators as potential CF therapeutics.³⁰

RESULTS

CFTR was modeled using a combination of restrained homology modeling and ROSETTA refinement.³¹ In the first modeling stage, ten initial outward-facing models with chloride ion columns inserted in their respective pores were generated by homology modeling based on the Sav1866 template. Given the low sequence similarity at the TM domains between CFTR and the available structural templates (<14% identity in the TMDs), detection and pairwise alignment of TM helices was performed by consensus analysis of several prediction methodologies, combined with evolutionary conservation and hydrophobicity analysis (see the Methods section and the SI).

In the second modeling stage, carefully designed constrained ROSETTA refinement was applied to three of the best outward facing structures, effectively transforming them into more channel-like compact conformations while refraining from collapsing their pores (Figure 2 and Methods section). This was achieved by the continued inclusion of respective chloride columns during the refinement process and involved the generation of 1200 different model structures in total.

Thirty models with the most favorable ROSETTA-score and channel-like structure (principally regarding TM salt-bridges and overall pore geometry calculated with HOLE2³³) were subsequently subjected to rigorous analysis according to the following criteria: (1) quality of experimentally suggested salt bridge and hydrogen-bond interactions (SI Table S1) as well as salt bridges restrained during modeling (see Methods section); (2) channel pore dimensions calculated with HOLE2 and comparison to experimental data; (3) degree of consistency with all pairwise distances derived from experimental cross-linking data (SI Table S2); (4) agreement with experimental residue accessibility data (SI Table S3).

The three best channel-like structures surviving these filters were further scrutinized by molecular docking. Five previously identified anionic open channel blockers (glibenclamide, NPPB, lonidamine, DNDS, TLCS) have been suggested experimentally to block the channel from the intracellular side, binding within the lower vestibule and forming ionic interactions with K95.²⁶ Two additional anionic blockers (mitiglinide and meglitinide) have also been found to block from the intracellular side but their ability to block K95 mutants has not been tested.³⁴ We docked all seven known open channel blockers (Figure 3) into the three alternative channel-pore structures using Glide^{35,36} (see Methods section). Of the three models, one was found to out-perform the other two in terms of producing experimentally supported blocker binding modes. Specifically, in this top performing model, pore-blocking poses were found in which ionic interactions are formed with K95.

Final Modeling Stage: Construction of an Integrated Model. The three surviving models showed different strengths and weaknesses when evaluated by all of the above criteria. Realizing that the conformational sampling procedure

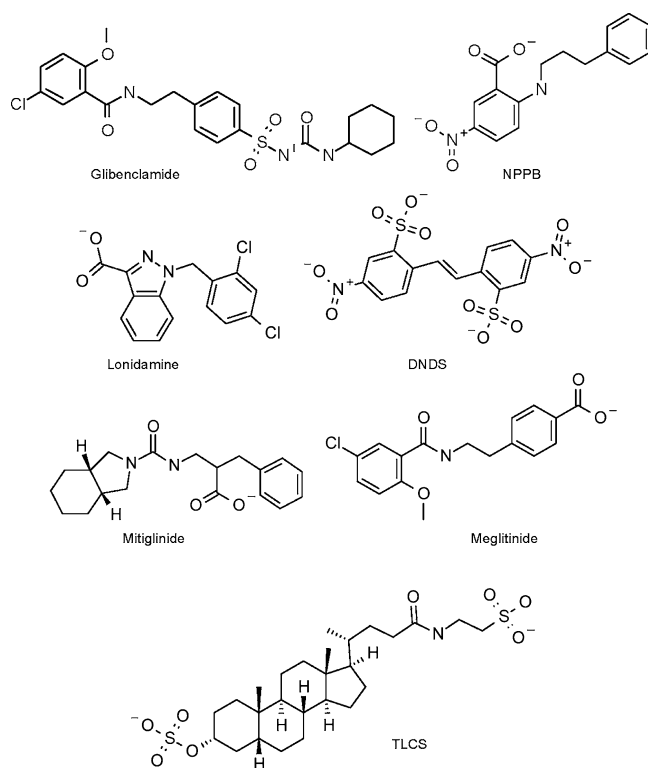


Figure 3. Structures of open channel blockers.

described above is not ergodic and strongly depends on initial conditions, an integrated model was constructed by combining the strong points of the two top scoring models. The third model was discarded as it was systematically out-performed by the other two.

CFTR model integration was accomplished using multi-template homology modeling with Prime,³⁶ with one model providing the template for TM10, TM11, and interconnecting loop (better agreement with F508 related distance constraints), and the other providing a template for the rest of the structure (superior blocker docking results). Using Prime ensured that the respective sidechain orientations from each of the two templates were preserved in the combined model. Prime sidechain refinement was performed on the grafted TM10–TM11 and proximal residues (using a 3 Å cutoff) to relieve unfavorable contacts at the seam line between template structures.

Evaluation of the Integrated Model. The final integrated model was re-evaluated using the above criteria. In this model, the expected channel topology is clearly visible (Figure 4) with the narrowest region about 4.5 Å in diameter, which is in line with a previously made suggestion of ~5 Å.²³ The outer vestibule is dominated by R334 as previously suggested by Smith et al.²⁸ and by Linsdell.^{26,27} Narrowing starts cytosolically to T338 (TM6) in agreement with the results of Alexander et al.²³ and Norimatsu et al.,²⁴ progresses through the selectivity conferring S341 (TM6), and culminates at M348 (TM6). The narrowest region of the modeled pore stretches down to W1145 (TM12) and is dominated by the following pore-lining residues: TM6 residues I344, V345, and M348, which were found to be of limited accessibility to thiol-reactive probes²³ (SI Table S3), TM12 residues S1141 and M1137, which were suggested as pore-lining,^{37,38} Ser877 (TM7) and W1145 (TM12) for which no functional data has so far been published,

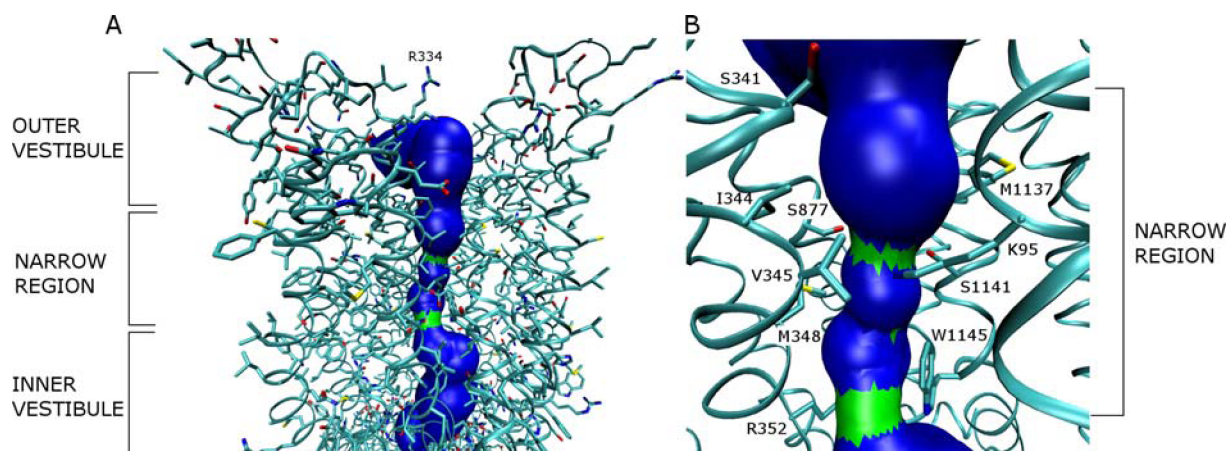


Figure 4. Modeled pore of CFTR visualized with VMD.³² (A) Transmembrane region divided into outer and inner vestibules separated by a narrow region. The protein is shown in cyan (as ribbons and sidechains), and the predicted pore (calculated with HOLE2) is shown in blue (pore diameter > 4.6 Å) and green (pore diameter < 4.6 Å). (B) Narrow region starts cytosolically to T338 at approximately S341 and reaches W1145 at the intracellular side. A minimal pore diameter of ~4.5 Å is obtained between residues K95, V345, S877, and S1141.

and the structural R352, forming a salt bridge with D993.³⁹ Widening of the inner vestibule begins cytosolically to W1145.

NBD1 and NBD2 are observed to be in a tight head-to-tail conformation (Figure 5) in compliance with experimental cross-linking data (SI Table S2), and the predicted hydrogen-bond between R555 (NBD1) and T1246 (NBD2)⁴⁰ is clearly observed (SI Table S1).

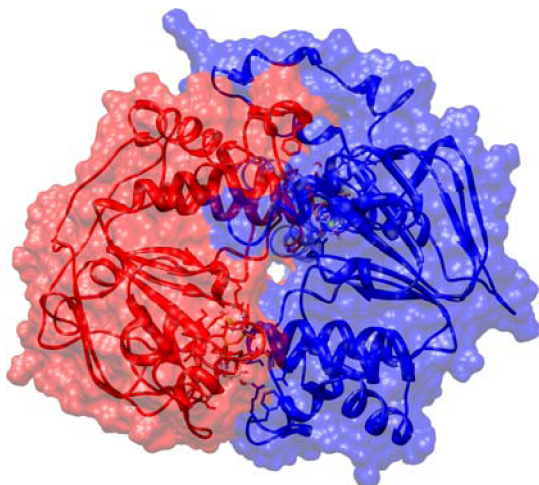


Figure 5. NBD1 (in blue) and NBD2 (in red) of the CFTR model, visualized with CHIMERA.⁴¹ A tight head-to-tail NBD configuration, which is necessary for the active state, is observable.

TM6 Accessibility. Due to the important contribution of TM6 to pore structure and function, a solvent accessibility assessment of TM6 residues was performed. Twenty-four TM6 residues were individually mutated to Cysteine in a sequential manner using Maestro,³⁶ followed by NACCESS⁴² calculations on each mutant. The accessibility of the SG atom was then compared with experimental results describing the reactivity of each cysteine with thiol reactive probes. Setting a cutoff of 20 Å² to predict experimental accessibility based on the NACCESS calculation results in good predictive power with a true positive rate = 0.6 and a true negative rate = 1 (Table 1). This prediction scheme classifies 9 out of 11 positions of limited accessibility as inaccessible. Since these positions can only be

Table 1. Atom Accessibility of Mutant Cysteine SG Atoms^a

residue number	experimental data (SI Table S3)	atom accessibility [Å ²]	predicted reactivity
330	unreactive	15	unreactive
331	limited	19	unreactive
332	unreactive	19	unreactive
333	limited	11	unreactive
334	REACTIVE	57	REACTIVE
335	REACTIVE	41	REACTIVE
336	limited	1	unreactive
337	limited	30	REACTIVE
338	REACTIVE	45	REACTIVE
339	limited	0	unreactive
340	limited	4	unreactive
341	limited	18	unreactive
342	limited	19	unreactive
343	unreactive	0	unreactive
344	limited	5	unreactive
345	limited	10	unreactive
346	unreactive	7	unreactive
348	limited	17	unreactive
349	limited	2	unreactive
350	unreactive	0	unreactive
351	unreactive	10	unreactive
353	limited	44	REACTIVE

^aReactive: susceptible to covalent modification by MTS reagents. Limited: reactive only to small permeant probes (dicyanides like [Ag(CN)₂]⁻ and [Au(CN)₂]⁻). Unreactive: does not react with any of the tested probes. Predicted reactivity is based on a 20 Å² atom accessibility cutoff. These predictions correspond to a true positive rate = 0.6 and a true negative rate = 1.

modified by small permeant probes, we believe this can still be viewed as providing a good estimate of channel dimensions.

Binding Modes of Open Channel Blockers. When docking the seven open channel blockers, highly overlapping pore blocking binding modes are obtained in the integrated model, forming ionic interactions with K95 (Figure 6) (top-scoring pose except number 3 for meglitinide and number 2 for NPPB and DNDS). This is in excellent agreement with the experimentally proposed mode of interaction for glibenclamide, NPPB, lonidamine, DNDS, and TLCS.²⁶ In addition, this

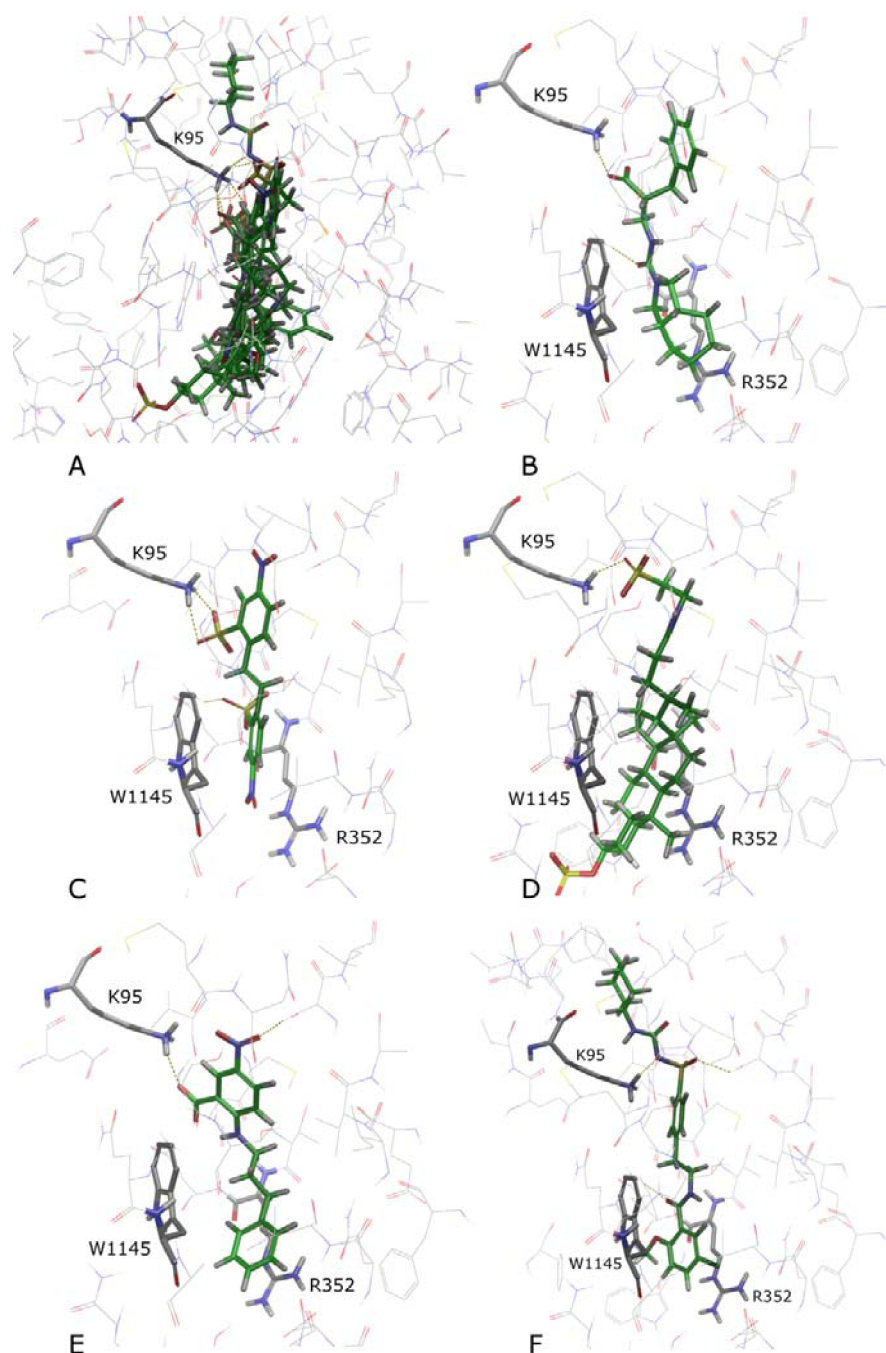


Figure 6. Binding modes of open channel blockers docked into the channel pore without constraints: (A) open channel blockers superimposed; (B) mitiglinide; (C) DNDS; (D) TLCS; (E) NPPB; (F) glibenclamide. Common interactions are observed with K95, W1145, and R352 (labeled). Dashed lines indicate hydrogen bonding interactions.

provides a functional prediction for mitiglinide and meglitinide, which are known to block from the intracellular side but have not yet been tested for interaction with specific amino acids.³⁴ All of the docked open channel blockers also share an aromatic/hydrophobic interaction with W1145 and a cation- π /hydrophobic interaction with R352. While R352 has an important structural role, no functional data is yet available for W1145. Additional residues implicated in individual blocker binding are S877 and Q353.

Virtual Screening. A virtual screening (VS) enrichment experiment was performed in order to test the model's ability to discriminate known open channel blockers from a set of

random compounds. First, a database was built by extracting 1643 random drug-like compounds, all possessing at least one negatively charged chemical group (common to known blockers and potentially essential for interaction with K95), from the diverse Maybridge screening collection.⁴³ The following chemical property ranges were used in library focusing: MW < 600 (the known blockers range from 300 to 560 Da), hydrogen-acceptors ≤ 10 (known blockers ranging from 3 to 10), hydrogen-donors ≤ 5 (known blockers ranging from 0 to 2), and number of negatively charged groups ≥ 1 (known blockers ranging from 1 to 2). This ensured "drug likeness" but also allowed significant diversity inherent to the

library to be maintained. Second, the seven known open channel blockers (Figure 3) were added to the database. Compound preparation, filtering, and docking of the 1643 decoy molecules in the database were performed as described in Methods, in an identical manner to that done for the seven known blockers. A single pore-blocking pose interacting with K95 was extracted for each docked compound using constraints incorporated into Glide and implemented postdocking. These constraints included a requirement for ionic interaction with K95 and a set of 3 Å spherical positional constraints defined along the chloride column (see Methods section). The constraints were first applied to the seven known blockers and proved capable of extracting the best pose previously obtained in the unconstrained docking run.

In addition to the seven known blockers, 1438 compounds out of the 1643 compound library survived the pose filter after initial screening; the rest did not have an ionic interaction with K95 or did not adopt a pore blocking pose. Both Glide GScore and a score measuring the Coulombic interaction with K95 produced efficient enrichments of the known blockers (Figures 7A and 7B, respectively), with respective $EF_{100\%}$ values of 1.7 and 5.4 (enrichment factor = fraction of actives found/fraction of library, with $EF_{100\%}$ corresponding to the retrieval of 100% of the known blockers). An even better enrichment was obtained with a consensus scoring approach, applying cutoffs based on the scores obtained for the known blockers: (1) Glide Score <

$-5.0 \text{ kcal mol}^{-1}$; (2) Coulombic interaction energy with K95 < -44 kJ mol^{-1} . Merely 226 library compounds (15.6%) survived this new screening filter, including all of the known blockers. This corresponds to an $EF_{100\%}$ of 6.3 with all known compounds found within 15% of the screened library. This suggests the model has a significant discriminatory ability in selecting for active compounds.

Molecular Dynamics Simulation. The model was subjected to a 75 ns MD simulation in an explicit, hydrated, lipid bilayer. The system was first equilibrated for 30 ns with a restrained chloride column maintained in the pore (see MD simulations in Methods). Since the number of chloride ions that pass simultaneously through the CFTR pore is not known, we assumed that they pass through the channel one at a time, and modeled the chloride column as having a single ionic charge distributed along the 20 comprising ions (see MD simulations in Methods). At the end of this simulation phase, the chloride column was removed and the system was equilibrated with gradually reducing constraints on the protein backbone for 15 ns allowing for the progressive formation of a water column solvating the pore (see Methods). This was followed by a final 30 ns unconstrained production run. During production, the channel was observed to undergo gradual structural reorganization, mainly involving the motion of pore-lining sidechains and their interaction with the unconstrained water column. The backbone of the TMs showed only minor fluctuation and appeared to stabilize over the course of the simulation, suggesting convergence may have been reached (SI Figure S5). As a result of these structural changes, the narrow selectivity-conferring region was seen to extend in length toward the outer vestibule, reaching a maximum length of two helical turns with an approximate diameter of 4 Å at its narrowest point (Figure 8). Several residues were observed to line the narrow region of the pore with the most significant being S341, I344, and V345 of TM6; T1134, M1137, N1138, and S1141 of TM12; L881 of TM8; and P99 of TM1. The location of these particular residues is mostly in agreement with experiment, which suggests that all are pore-lining^{23,37,38} (and conductance modulating in the case of P99⁴⁴ and S341^{45,46}). The exceptions are L881 for which there is no information, and N1138 where our results are in conflict with data that implies this residue does not have a pivotal role in the pore.³⁷

K95 lies at the entrance of the narrow region on the inner-vestibule side and may play a role in attracting chloride ions into the selectivity-conferring zone.²⁶ The simulation reveals that neighboring E92 may play a role in modulating conductance by competing with chloride ions for interaction with K95. During the simulation, a change in the channel conformation with respect to the starting structure was observed in the outer vestibule, with TM1 and TM6 moving closer together, reducing the diameter of the pore in the vicinity of F337 and T338 from 8.6 to 4.9 Å. During this shift, F337 and T338 also maintained their solvent accessibility, making them likely to be involved in anion selectivity as experimental data suggests.^{47,48} In addition, the maximal outer-vestibule pore diameter (as measured adjacent to R334) was reduced from 9.8 to 5.9 Å. However, the maximal inner-vestibule pore diameter remained more consistent, shifting from only 9.5 to 8.2 Å. Regarding the overall channel structure, the five salt-bridges restrained during initial modeling (experimentally supported salt-bridges R352-D993³⁹ and R347-D924,⁴⁹ as well as R134-E1104, R1102-D1154, and D873-R933) all remained stable and intact during the simulation.

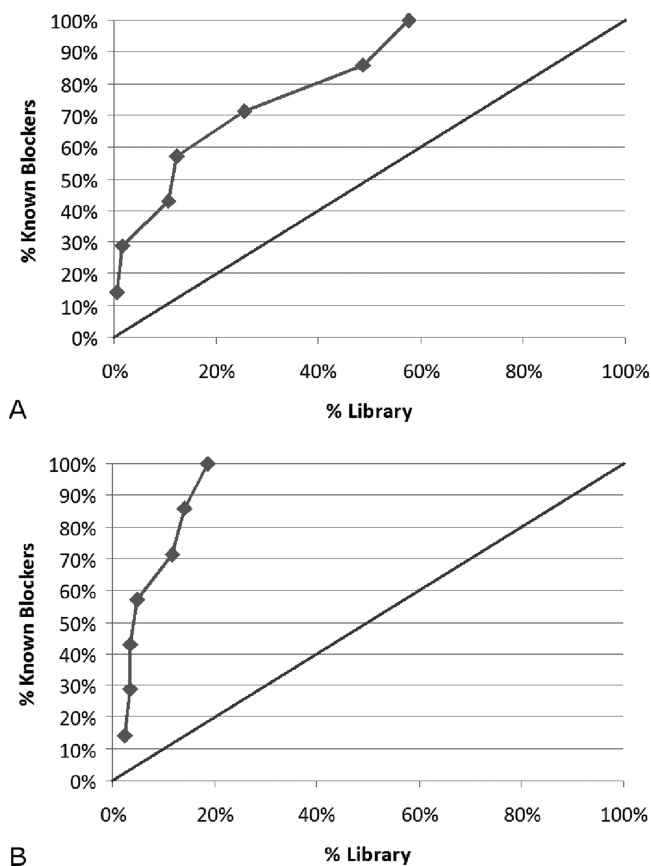


Figure 7. Enrichment graphs for the retrieval of seven known CFTR inhibitors among a library of 1643 random drug-like compounds (lines with points) enrichment of known blockers by virtual screening; (straight lines without points) retrieval of known blockers by random selection only. (A) Enrichment by Glide GScore. (B) Enrichment by K95 Coulombic interaction.

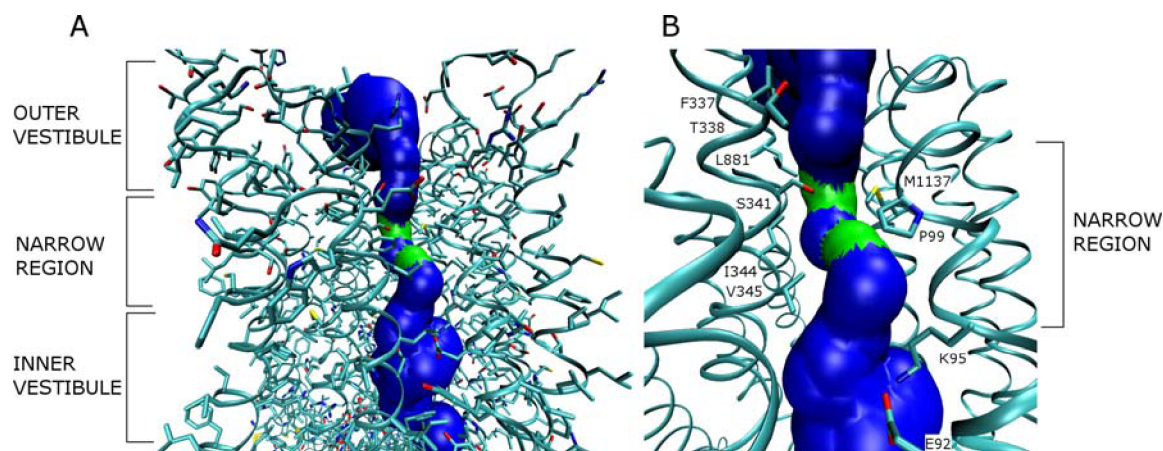


Figure 8. Modeled CFTR pore following 75 ns MD simulation, visualized with VMD.³² (A) Complete pore containing three distinct structural compartments. (B) Narrow region of the pore. The likely selectivity filter encompasses the two green bands, where the pore diameter narrows to ~ 4.0 Å. The protein is shown in cyan, and the predicted pore (calculated with HOLE2) is shown in blue (pore diameter > 4.6 Å) and green (pore diameter < 4.6 Å).

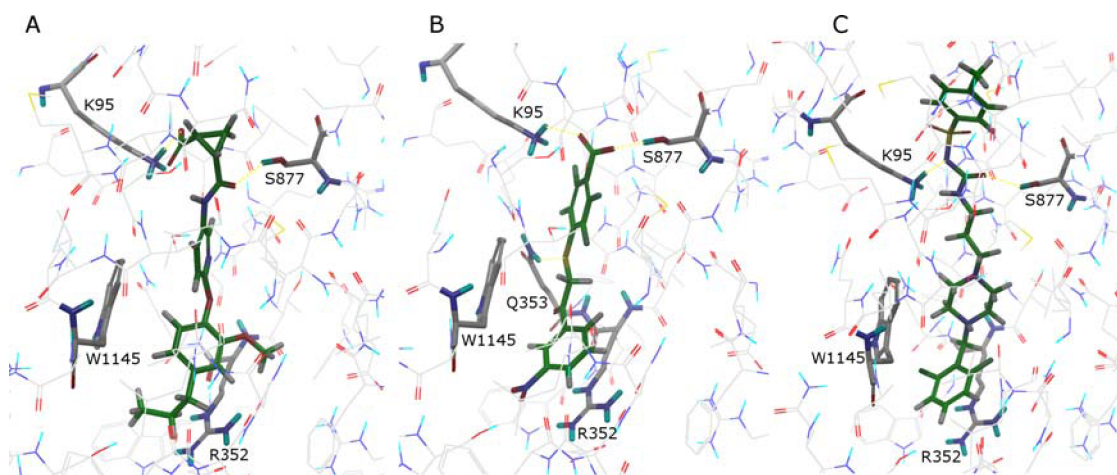


Figure 9. Examples of high-scoring library compounds discovered during virtual screening: (A) Maybridge BTB09406; (B) Maybridge BTB08329 (benzoic acid); (C) Maybridge AW01120 (sulfonylurea).

DISCUSSION

The current model of CFTR agrees with previously proposed channel properties, including a distinct outer vestibule followed by a narrow selectivity-conferring region and an inner vestibule wide enough to accommodate open channel blockers. This is in contrast to previously published models that have been made publicly available, which present CFTR in the outward-facing Sav1866-based conformation corresponding to a wide barrel-shaped channel pore. This observation may not be applicable to the models reported by Alexander et al.²³ and Norimatsu et al.,²⁴ which were generated by MD refinement (5 and 30 ns simulations, respectively, the latter being published while our study was under review) of the same Sav1866-based outward-facing homology model. However, as neither the sequence alignment to Sav1866 nor the coordinates of either model was made available to the public, proper evaluation of their respective architectures is impossible. Having said that, of the two, the model of Norimatsu et al.²⁴ appears to be the closest to approximating the expected architecture of CFTR. However, as already mentioned, a possible drawback of this model is premature termination of the conductance path on the cytoplasmic side, as well as a tendency toward being too narrow in the selectivity-conferring region.²⁴ This is something

that we took great care to avoid in our CFTR model by introducing a chloride column into our modeling scheme. Thus, our model contains both a cytoplasmic point of entry and a selectivity-conferring region that is wide enough for the passage of chloride ions.

Our model provides insight into existing experimental data as well as novel predictions. From a structural perspective, the model and MD simulations propose structural and functional roles for several unaddressed residues. Especially interesting are five salt-bridge interactions suggested as important for the structural integrity of the channel-like conformation: R352-D993, R347-D924, R134-E1104, R1102-D1154, and D873-R933. While experimental evidence exists only for the first two, maintaining all five salt-bridges was found to have a positive effect on modeling outcome, where structures generated without these constraints agreed less well with experimental data as a whole. Importantly, the channel-like structure with outer vestibule, narrow region, and lower vestibule seems to require, at least in this modeling scheme, the presence of all five salt-bridges. In further support of this observation, all five salt-bridges also remained stable throughout unconstrained MD. Notably, a salt bridge between R134 and E1104 is supported by the finding that R134E/Q mutations are detrimental to channel

function.⁵⁰ Notably, both the R352-D993 and R347-D924 experimentally supported salt-bridge interactions are absent in the Serohijos et al. model,²⁰ while in the Mornon et al. model,²¹ only the R347-D924 salt-bridge exists (SI Table S1). The latter was also reported as missing from the Alexander et al. model,²³ and its status in the related Norimatsu et al. model²⁴ is unknown. In addition, an experimentally supported hydrogen-bond between R555 in NBD1 and T1246 in NBD2⁴⁰ is present in our model and is stable in simulation.

From a pharmacological perspective, our model reveals a common mechanism of inhibition by anionic open channel blockers, correlating with experimental results and predicting previously unaddressed interactions with pore residues. Furthermore, when tested in a virtual-screening enrichment experiment, our model performed well, suggesting that it might be reliable enough to be used as a template for discovery of novel open channel blockers, which are recognized as potential antidiarrheal therapeutics. Molecules from the Maybridge collection that score highly in this experiment show excellent pharmacophore overlap with the known blockers, suggesting that they could indeed be active as open channel blockers. Reassuringly, without the use of constraints imposing specific ligand chemistry, these compounds include chemical classes characteristic of CFTR channel blockers, such as disulfonic stilbenes, sulfonyleureas, arylaminobenzoates, benzoic acid derivatives, and 3-phenylpropionic acid derivatives.^{34,51} Three such examples of high-scoring library compounds are shown in Figure 9.

On the down side, recent experimental results, published after this work was completed, expose a limitation of the current model and modeling approach. The recent publication suggests a cross-linking distance of 7–8 Å between I344 and both K95 and K98.⁵² In contrast, inter-residue distances in our model are 11.6 and 15.3 Å for K95-I344 and K98-I344, respectively, suggesting slightly different relative orientations of TM1 and TM6.

This reflects the inherent level of difficulty in modeling a channel-like conformation of CFTR from the Sav1866-based outward-facing conformation. On the one hand, the Sav1866-based conformation is not necessarily accessible to CFTR. On the other hand, the template TM region is inherently flexible, having to transition between open and closed conformations. The combination of these two issues suggests that obtaining conformational convergence would be hard and could rely heavily on modeling conditions, e.g. the experimental constraints incorporated into the modeling procedure. While we have obtained a conformation that seems to be in better agreement with experimental data than previously reported models that can be evaluated, particularly in terms of overall channel geometry and the potential for chloride ion passage, it may not be the most accurate conformation or, alternatively, it may be one of several conformations accessible to functional CFTR: a concept that is supported by recent experiments.⁵³ Indeed, it is also possible that some of the other published models of CFTR adopt conformations that are physically accessible, corresponding to varying degrees of conductance. We expect that as more structurally interpretable experimental data referring to the conducting state of CFTR becomes available our modeling method could be used to derive models that are increasingly more accurate.

Our method is also limited by the approximations inherent to the use of classical ROSETTA, which assumes solvation in water, and we realize that results may improve following future

transitioning to newer versions of ROSETTA capable of handling a membrane environment. Still, this may not have had a critical effect on the modeling outcome given the constrained nature of the refinement and in light of the clear agreement with a large bulk of experimental data.

Finally, because the outward facing Sav1866-based conformation is not necessarily realistic for CFTR, it is unclear whether physically realistic and computationally demanding MD simulations, such as those used by Alexander et al.²³ and Norimatsu et al.,²⁴ are a good algorithmic choice. Our less CPU intensive modeling approach essentially provides an experimentally guided conformational search mechanism, which could be followed by full blown MD refinement in an explicit lipid bilayer once the structure is much closer to its target conformation. This might be a more adequate approach in this particular case.

CONCLUSIONS

A channel-like model of CFTR, which may represent an ion conducting conformation, was developed through a unique modeling protocol and validated with a broad range of experimental data. MD simulations of the model proposed residues that are likely to be involved in conferring ion selectivity in the pore. Novel functional roles for CFTR residues were also suggested, including salt-bridge formation with potential structural significance and interaction with open channel blockers. It was further demonstrated that the model could potentially be utilized for drug discovery of CFTR inhibitors that could ultimately impact the development of treatments for AWD. The coordinates of our pre-MD model are provided in the Supporting Information.

METHODS

Prediction of TM Helices and Pairwise Alignments. We approximated the location of the TM helices in the sequence of CFTR using the TMHMM,⁵⁴ HMMTOP,⁵⁵ SPLIT4,⁵⁶ and PSIPRED⁵⁷ algorithms. Since CFTR is distantly related to Sav1866, direct sequence alignment could not accurately match the two sequences. We therefore utilized three profile-to-profile fold recognition methods to obtain sequence alignments between the TM domains of Sav1866 and those of CFTR, namely HMAP,⁵⁸ HHPRED,⁵⁹ and FFAS03.⁶⁰ Core segments of TM helices were first identified by integrating the results from the profile-to-profile alignment methods, secondary structure, and TM predictions. Subsequently, the precise helical boundaries were determined by incorporating data derived from evolutionary conservation and hydrophobicity analysis of a collection of ABC C subfamily sequences (see the SI).

Sequence Data and Evolutionary Conservation Analysis. The phylogenetic analysis by Jordan et al.⁶¹ found that 11 other ABCC human proteins, exhibiting the same domain organization as CFTR, are CFTR's closest homologues in the human proteome. This study showed that three human ABCB proteins, which reside on a separate branch on the phylogenetic tree, also encompass two TMDs and two NBDs on the same polypeptide chain. Relying on this analysis, we collected sequences identified by the Ensembl database⁶² as orthologues for these 14 human ABCC and ABCB proteins. We then excluded fragments, aligned the remaining sequences with MAFFT,⁶³ and constructed a phylogenetic tree using PHYML.⁶⁴ Using the phylogenetic tree, we observed that the proteins belonging to the ABCB subfamily were significantly

distant from the ABCC subfamily. Therefore, we included in the final multiple sequence alignment (MSA) only the 177 sequences belonging to the ABCC subfamily. This MSA was used to compute evolutionary conservation scores with ConSurf⁶⁵ (see the SI).

Structural Modeling. 1. *Homology Modeling.* Core segments of TM helices were identified by manually integrating the results of several profile-to-profile alignment methods, as well as secondary structure prediction and TM prediction algorithms. Subsequently, data from evolutionary conservation and hydrophobicity analyses of a collection of ABCC subfamily sequences were used to fine-tune the TM boundaries based on the following conventions: (1) residues comprising the protein core (e.g., interhelical interfaces) of TM proteins tend to be conserved^{66–69} while residues facing the membrane are in most cases less vital to protein function and are thus mostly variable; (2) TM helices must possess a strong hydrophobic signal to insert into the membrane, sequestering polar and charged residues from contact with the lipid tails (see the SI for details).

CFTR was modeled by homology to Sav1866 without the R-region (residues 650–846) because no structural template corresponding to this section could be clearly identified. Two crystal structures of Sav1866 are available: 2HYD, Sav1866 in complex with ADP, and 2ONJ, Sav1866 in complex with AMP-PMP. These are distinguished by slight conformational changes in the region of the bound nucleotide. 2ONJ was selected as the template for homology modeling since the ATP analog AMP-PMP more closely resembles ATP, the ligand bound to CFTR in its conducting state.

An initial homology model was built with MODELLER⁷⁰ using a multiple templating approach combining the structure of Sav1866 with the higher resolution structure of the *wt* human CFTR NBD1 fragment (2PZE). The following constraints were used in modeling: (1) distance constraints imposing the experimentally proposed salt-bridges: R352-D993³⁹ and R347-D924;⁴⁹ (2) distance constraints imposing salt-bridges inferred from structural analysis of initial models generated without these constraints: R134-E1104, R1102-D1154, and D873-R933; (3) helical constraint on the TM11 insertion required to preserve pairwise distances between F508 and neighboring residues as proposed by cross-linking experiments²⁰ (SI Table S2); (4) helical constraint on TM8 to prevent unwinding due to the deletion required for D924 reorientation; (5) distance restraints between MG and ATP with the following residues: H1402, E1371, K1250, D1370, and S1251, comprising the ATP binding-site of NBD2, thus ensuring they match their corresponding catalytic residues in Sav1866; (6) distance restraints between pairs of residues that are known to associate in experimental cross-linking studies: 340–877,⁷¹ 348–1142,⁷² 351–1142,⁷² 95–1141,⁷³ 356–1145,⁷² 508–1068,²⁰ 508–1074.²⁰

A chloride ion column was inserted into the pore of the template structure of Sav1866, which was then made rigid during the modeling process. This was found necessary to prevent the collapse of the channel pore during the next stages of refinement. The column was placed in line with the Z-axis, at X and Y equal to zero according to the 2ONJ coordinate system in the OPM database.⁷⁴ Cl[−] atoms were placed at a spacing equivalent to their vdW diameter, equating to a total of 36 Cl[−] ions in the column.

Five crystallographic water molecules, identified by their conservation in crystal structures of NBD1 and other homologous NBDs, as well as relatively low B-factors, were

included in the NBD1 and NBD2 models, as previously described.³⁰

The regulatory insertion (RI) loop of NBD1 (residues 404–435), which is not observable in full in any of the available crystal structures of NBD1, was modeled based on the previously generated model of Mornon et al.²¹ The RI loop was excised from the Mornon et al. model, superimposed onto 2PZE, and incorporated into the model by MODELLER multiple templating.

Ten models were generated with MODELLER with slow refinement and twenty cycles of simulated annealing. Of these, three were selected for further refinement, based on visual inspection of the salt-bridge and pore-lining residues.

2. *ROSETTA Refinement.* TM and NBD2 regions of three different models were refined using the ROSETTA v3.1 “Fast Relax” refinement procedure,³¹ while keeping the backbone of NBD1 frozen (except for the regulatory insertion loop) and applying sidechain restraints to the same salt-bridges that were restrained during model building (initial tests showed that this procedure tends to generate a collapsed pore, leading to the inclusion of a manually positioned Cl[−] column in the center of the channel, as described in Methods). However, due to the nature of the applied restraints, which were rotamer-based rather than distance-based, salt-bridge interactions were favored but not necessarily enforced in each of the generated models.

A total of 1200 ROSETTA conformations were generated (400 for each MODELLER output structure) and then subjected to filtering based on salt-bridge interactions. Merely 170 models passed this filtering stage, all belonging to the same conformational cluster (3 Å cutoff used for C α clustering in ROSETTA). Analysis showed that with 400 ROSETTA conformations per MODELLER model, sampling is converged (results not shown). These models already show a more compact arrangement of the TM bundle transforming the outward-facing conformation into a more channel-like structure (e.g., see Figure 2).

Thirty top-scoring ROSETTA models (also showing best salt-bridge conformations) were subsequently subjected to energy minimization in MacroModel.³⁶

3. *MacroModel Minimization of ROSETTA Models.* A maximum of 10 000 cycles of PRCG minimization was performed on each model using the OPLS2005 force-field and a distance-dependent dielectric of 4. This is a trade-off between vacuum and water dielectrics, which may be more suitable for a membrane protein and is chosen here in the absence of an implicit-membrane model in MacroModel. Constraints were placed on protein dihedral angles and the position of ATP and MG atoms. Distance constraints were applied to TM salt bridges, with the Cl[−] column frozen.

Docking. 1. *Ligand Preparation.* Compounds were prepared for docking using the ligand preparation option in Schrödinger Virtual Screening Workflow.³⁶ The regularize geometry option was selected, and Ionizer was used for generating tautomers and protonation states at pH = 7.0 ± 1.0. Ligands for enrichment analysis were extracted from the Maybridge collection using the filtering option in VSW and the following criteria: MW < 600 (known blockers range from 300 to 560 Da), hydrogen-acceptors ≤ 10, hydrogen-donors ≤ 5, number of negatively charged chemical groups ≥ 1.

2. *Glide Protocol.* In docking, amide bond conformations were constrained to the input geometries, strain energy correction was applied, postdocking minimization was performed for the top five poses, and at most five poses were

reported for each ligand. During constrained docking, [N-] was added to the default charged acceptor SMARTS patterns to account for glibenclamide charge. An inner box size of $12 \times 12 \times 14$ was used, centered at the midpoint between K95 and W1145 (selected following multiple tests with different box sizes and positions).

Molecular Dynamics Simulation. A 75 ns MD simulation was performed on the model of CFTR using NAMD⁷⁵ and the CHARMM-27 force-field⁷⁶ with 192 CPUs on the HECTOR Supercomputer. System setup was performed in VMD.³² A POPC membrane was added using the MEMBRANE package and the system was solvated with TIP3P water using SOLVATE. Fourteen Cl⁻ ions were added into the surrounding solvent environment to neutralize the system, and salt was added at a concentration of 0.15 M. The system was initially relaxed with four cycles of minimization followed by a 2.5 ns MD run, with harmonic restraints on the protein progressively relieved across the four cycles from 10 to 0 kcal mol⁻¹ Å⁻². The system was subsequently equilibrated for 30 ns, with 20 Cl⁻ ions of the original 36 Cl⁻ ion column maintained in the model, filling the channel pore from top of the outer vestibule to bottom of the inner vestibule. The ion charge was reduced to -0.05 so that the total charge would not exceed that of a single passing ion. The ions in the Cl⁻ column were harmonically constrained using a 1 kcal mol⁻¹ Å⁻² force constant. In a second equilibration phase, which lasted 15 ns, the chloride column was removed by converting the twenty chlorides of -0.05 charge into one centrally positioned unconstrained chloride ion with a normal charge of -1. This allowed the pore to become fully solvated, effectively forming an unconstrained water column. During this period, the backbone of the protein was harmonically constrained, employing a gradually reducing force constant of 1, 0.05, or 0 kcal mol⁻¹ Å⁻² as a water column was gradually formed. Sidechains were allowed to move freely throughout the equilibration period. Equilibration was followed by an unconstrained 30 ns production run.

Here, rmsd calculations were made using the "rmsd Trajectory Tool" in VMD as well as an in-house program for calculating rmsd per residue. Plots were made with GNUPLLOT.⁷⁷

Pore Analysis. HOLE2³³ was used to measure the dimensions of the model pore and was executed with default parameters, except for the following: "endrad" parameter set to 10.0, "cvect" specified as the Z-axis, i.e. the direction of the pore, and "cpoint" set as the coordinates of the most central pore chloride ion.

■ ASSOCIATED CONTENT

📄 Supporting Information

Sequence alignment, additional details of the alignment methodology, salt-bridge analysis in current and previously published models, analysis of experimentally derived pairwise distances in current and previous models, functional and solvent accessibility data for TM6 residues, coordinates of the pre-MD model, additional analysis of MD. This information is available free of charge via the Internet at <http://pubs.acs.org>.

■ AUTHOR INFORMATION

Corresponding Author

*E-mail: jordi.villa@uvic.cat. Phone: +34938815519 (J.V.-F.). E-mail: nirb@tauex.tau.ac.il. Phone: +97236406709 (N.B.T.).

Author Contributions

[†]These authors contributed equally to the article.

Notes

The authors declare no competing financial interest.

■ ACKNOWLEDGMENTS

J.D. and J.V.-F. acknowledge Ignasi Buch for help in obtaining Figure 2. This work has also been partially funded by grants TSI-020110-2009-431, CTQ2008-00755, and BFU2006-28430-E/BMC, as well as supported by the Israel Science Foundation Grant 1331/11 (N.B.T.). M.S. was supported by the Edmond J. Safra Bioinformatics program at Tel Aviv University. In addition, we acknowledge the UK Supercomputing Service (HECTOR). The GRIB is a node of the Spanish National Institute of Bioinformatics (INB) and member of the COMBIOMED network (RD07/0067/0001) and the virtual physiological human (VPH) NoE (FP7-ICT-2007-2-223920).

■ ABBREVIATIONS:

CFTR, cystic fibrosis transmembrane conductance regulator; CF, cystic fibrosis; MD, molecular dynamics; AWD, acute water diarrhea; ABC, ATP-binding cassette; MSD, membrane spanning domain; ICL, intracellular loop; NBD, nucleotide binding domain; TM, transmembrane

■ REFERENCES

- (1) O'Sullivan, B. P.; Freedman, S. D. Cystic fibrosis. *The Lancet* **2009**, *373*, 1891–1904.
- (2) de Hostos, E. L.; Choy, R. K.; Nguyen, T. Developing novel antisecretory drugs to treat infectious diarrhea. *Future Med. Chem.* **2011**, *3*, 1317–1325.
- (3) *Diarrhoea: why children are still dying and what can be done*; World Health Organization. 2009, ISBN 978-92-806-4462-3 (UNICEF).
- (4) Riordan, J. R.; Rommens, J. M.; Kerem, B.; Alon, N.; Rozmahel, R.; Grzelczak, Z.; Zielenski, J.; Lok, S.; Plavsic, N.; Chou, J. L. Identification of the cystic fibrosis gene: cloning and characterization of complementary DNA. *Science* **1989**, *245*, 1066–1073.
- (5) Pilewski, J. M.; Frizzell, R. A. Role of CFTR in airway disease. *Physiol. Rev.* **1999**, *79*, S215–S255.
- (6) Davis, P. B. Cystic fibrosis since 1938. *Am. J. Resp. Crit. Care Med.* **2006**, *173*, 475–482.
- (7) Sheppard, D. N.; Welsh, M. J. Structure and function of the CFTR chloride channel. *Physiol. Rev.* **1999**, *79*, S23–S45.
- (8) Gadsby, D. C.; Nairn, A. C. Control of CFTR channel gating by phosphorylation and nucleotide hydrolysis. *Physiol. Rev.* **1999**, *79*, S77–S107.
- (9) Du, K.; Lukacs, G. L. Cooperative assembly and misfolding of CFTR domains in vivo. *Mol. Biol. Cell* **2009**, *20*, 1903–1915.
- (10) Du, K.; Sharma, M.; Lukacs, G. L. The DeltaF508 cystic fibrosis mutation impairs domain-domain interactions and arrests post-translational folding of CFTR. *Nat. Struct. Mol. Biol.* **2005**, *12*, 17–25.
- (11) Thibodeau, P. H.; Brautigam, C. A.; Machius, M.; Thomas, P. J. Side chain and backbone contributions of Phe508 to CFTR folding. *Nat. Struct. Mol. Biol.* **2005**, *12*, 10–16.
- (12) Wang, C.; Protasevich, I.; Yang, Z.; Seehausen, D.; Skalak, T.; Zhao, X.; Atwell, S.; Spencer Emtage, J.; Wetmore, D. R.; Brouillette, C. G.; Hunt, J. F. Integrated biophysical studies implicate partial unfolding of NBD1 of CFTR in the molecular pathogenesis of F508del cystic fibrosis. *Protein Sci.* **2010**, *19*, 1932–1947.
- (13) Protasevich, I.; Yang, Z.; Wang, C.; Atwell, S.; Zhao, X.; Emtage, S.; Wetmore, D.; Hunt, J. F.; Brouillette, C. G. Thermal unfolding studies show the disease causing F508del mutation in CFTR thermodynamically destabilizes nucleotide-binding domain 1. *Protein Sci.* **2010**, *19*, 1917–1931.
- (14) Riordan, J. R. CFTR function and prospects for therapy. *Annu. Rev. Biochem.* **2008**, *77*, 701–726.

- (15) Ma, T.; Thiagarajah, J. R.; Yang, H.; Sonawane, N. D.; Folli, C.; Galiotta, L. J.; Verkman, A. S. Thiazolidinone CFTR inhibitor identified by high-throughput screening blocks cholera toxin-induced intestinal fluid secretion. *J. Clin. Invest.* **2002**, *110*, 1651–1658.
- (16) Sonawane, N. D.; Verkman, A. S. Thiazolidinone CFTR inhibitors with improved water solubility identified by structure activity analysis. *Bioorg. Med. Chem.* **2008**, *16*, 8187–8195.
- (17) Yang, B.; Sonawane, N. D.; Zhao, D.; Somlo, S.; Verkman, A. S. Small-molecule CFTR inhibitors slow cyst growth in polycystic kidney disease. *J. Am. Soc. Nephrol.* **2008**, *19*, 1300–1310.
- (18) Tradtrantip, L.; Sonawane, N. D.; Namkung, W.; Verkman, A. S. Nanomolar potency pyrimido-pyrrolo-quinolinedione CFTR inhibitor reduces cyst size in a polycystic kidney disease model. *J. Med. Chem.* **2009**, *52*, 6447–6455.
- (19) Kopeikin, Z.; Sohma, Y.; Li, M.; Hwang, T. C. On the mechanism of CFTR inhibition by a thiazolidinone derivative. *J. Gen. Physiol.* **2010**, *136*, 659–671.
- (20) Serohijos, A. W.; Hegedus, T.; Aleksandrov, A. A.; He, L.; Cui, L.; Dokholyan, N. V.; Riordan, J. R. Phenylalanine-508 mediates a cytoplasmic-membrane domain contact in the CFTR 3D structure crucial to assembly and channel function. *Proc. Natl. Acad. Sci. U.S.A.* **2008**, *105*, 3256–3261.
- (21) Mornon, J. P.; Lehn, P.; Callebaut, I. Atomic model of human cystic fibrosis transmembrane conductance regulator: membrane-spanning domains and coupling interfaces. *Cell. Mol. Life Sci.* **2008**, *65*, 2594–2612.
- (22) Mornon, J. P.; Lehn, P.; Callebaut, I. Molecular models of the open and closed states of the whole human CFTR protein. *Cell. Mol. Life Sci.* **2009**, *66*, 3469–3486.
- (23) Alexander, C.; Ivetac, A.; Liu, X.; Norimatsu, Y.; Serrano, J. R.; Landstrom, A.; Sansom, M.; Dawson, D. C. Cystic fibrosis transmembrane conductance regulator: using differential reactivity toward channel-permeant and channel-impermeant thiol-reactive probes to test a molecular model for the pore. *Biochemistry* **2009**, *48*, 10078–10088.
- (24) Norimatsu, Y.; Ivetac, A.; Alexander, C.; Kirkham, J.; O'Donnell, N.; Dawson, D. C.; Sansom, M. Cystic fibrosis transmembrane conductance regulator: a molecular model defines the architecture of the anion conduction path and locates a "bottleneck" in the pore. *Biochemistry* **2012**, *51*, 2199–2212.
- (25) Dawson, R. J.; Locher, K. P. Structure of a bacterial multidrug ABC transporter. *Nature* **2006**, *443*, 180–185.
- (26) Linsdell, P. Location of a common inhibitor binding site in the cytoplasmic vestibule of the cystic fibrosis transmembrane conductance regulator chloride channel pore. *J. Biol. Chem.* **2005**, *280*, 8945–8950.
- (27) Linsdell, P. Mechanism of chloride permeation in the cystic fibrosis transmembrane conductance regulator chloride channel. *Exp. Physiol.* **2006**, *91*, 123–129.
- (28) Smith, S. S.; Liu, X.; Zhang, Z. R.; Sun, F.; Kriewall, T. E.; McCarty, N. A.; Dawson, D. C. CFTR: covalent and noncovalent modification suggests a role for fixed charges in anion conduction. *J. Gen. Physiol.* **2001**, *118*, 407–431.
- (29) Verkman, A. S.; Lukacs, G. L.; Galiotta, L. J. CFTR chloride channel drug discovery—inhibitors as antiarrheals and activators for therapy of cystic fibrosis. *Curr. Pharm. Des.* **2006**, *12*, 2235–2247.
- (30) Kalid, O.; Mense, M.; Fischman, S.; Shitrit, A.; Bihler, H.; Ben-Zeev, E.; Schutz, N.; Pedemonte, N.; Thomas, P. J.; Bridges, R. J.; Wetmore, D. R.; Marantz, Y.; Senderowitz, H. Small molecule correctors of F508del-CFTR discovered by structure-based virtual screening. *J. Comp.-Aided Mol. Des.* **2010**, *24*, 971–991.
- (31) Simons, K. T.; Bonneau, R.; Ruczinski, I.; Baker, D. Ab initio protein structure prediction of CASP III targets using ROSETTA. *Proteins* **1999**, *S3*, 171–176.
- (32) Humphrey, W.; Dalke, A.; Schulten, K. VMD: visual molecular dynamics. *J. Mol. Graph.* **1996**, *14*, 33–38.
- (33) Smart, O. S.; Goodfellow, J. M.; Wallace, B. A. The pore dimensions of gramicidin A. *Biophys. J.* **1993**, *65*, 2455–2460.
- (34) Cai, Z.; Lansdell, K. A.; Sheppard, D. N. Inhibition of heterologously expressed cystic fibrosis transmembrane conductance regulator Cl⁻ channels by non-sulphonylurea hypoglycaemic agents. *Br. J. Pharmacol.* **1999**, *128*, 108–118.
- (35) Friesner, R. A.; Banks, J. L.; Murphy, R. B.; Halgren, T. A.; Klicic, J. J.; Mainz, D. T.; Repasky, M. P.; Knoll, E. H.; Shelley, M.; Perry, J. K.; Shaw, D. E.; Francis, P.; Shenkin, P. S. Glide: a new approach for rapid, accurate docking and scoring. 1. Method and assessment of docking accuracy. *J. Med. Chem.* **2004**, *47*, 1739–1749.
- (36) *Glide*, version 9.5; Schrodinger, LLC: New York, NY, 2005.
- (37) Gupta, J.; Evagelidis, A.; Hanrahan, J. W.; Linsdell, P. Asymmetric structure of the cystic fibrosis transmembrane conductance regulator chloride channel pore suggested by mutagenesis of the twelfth transmembrane region. *Biochemistry* **2001**, *40*, 6620–6627.
- (38) Dawson, D. C.; Smith, S. S.; Mansoura, M. K. Asymmetric structure of the cystic fibrosis transmembrane conductance regulator chloride channel pore suggested by mutagenesis of the twelfth transmembrane region. *Physiol. Rev.* **1999**, *79*, S47–S75.
- (39) Cui, G.; Zhang, Z. R.; O'Brien, A. R.; Song, B.; McCarty, N. A. Mutations at arginine 352 alter the pore architecture of CFTR. *J. Membr. Biol.* **2008**, *222*, 91–106.
- (40) Vergani, P.; Lockless, S. W.; Nairn, A. C.; Gadsby, D. C. CFTR channel opening by ATP-driven tight dimerization of its nucleotide-binding domains. *Nature* **2005**, *433*, 876–880.
- (41) Pettersen, E. F.; Goddard, T. D.; Huang, C. C.; Couch, G. S.; Greenblatt, D. M.; Meng, E. C.; Ferrin, T. E. UCSF Chimera - a visualization system for exploratory research and analysis. *J. Comput. Chem.* **2004**, *25*, 1605–1612.
- (42) Hubbard, S. J.; Thornton, J. M. NACCESS, version 2.1.1, 1993; <http://www.bioinf.manchester.ac.uk/naccess>.
- (43) <http://www.maybridge.com/default.aspx>.
- (44) Ge, N.; Muise, C. N.; Gong, X.; Linsdell, P. Direct comparison of the functional roles played by different transmembrane regions in the cystic fibrosis transmembrane conductance regulator chloride channel pore. *J. Biol. Chem.* **2004**, *279*, 55283–55289.
- (45) McCarty, N. A.; Zhang, Z. R. Identification of a region of strong discrimination in the pore of CFTR. *Am. J. Physiol.* **2001**, *281*, L852–L867.
- (46) McDonough, S.; Davidson, N.; Lester, H. A.; McCarty, N. A. Novel pore-lining residues in CFTR that govern permeation and open-channel block. *Neuron* **1994**, *13*, 623–634.
- (47) Linsdell, P.; Zheng, S. X.; Hanrahan, J. W. Non-pore lining amino acid side chains influence anion selectivity of the human CFTR Cl⁻ channel expressed in mammalian cell lines. *J. Physiol.* **1998**, *512*, 1–16.
- (48) Linsdell, P. Inhibition of cystic fibrosis transmembrane conductance regulator chloride channel currents by arachidonic acid. *Can. J. Physiol. Pharmacol.* **2000**, *78*, 490–499.
- (49) Cotten, J. F.; Welsh, M. J. Cystic fibrosis-associated mutations at arginine 347 alter the pore architecture of CFTR. *J. Biol. Chem.* **1999**, *274*, 5429–5435.
- (50) Aubin, C. N.; Linsdell, P. Positive charges at the intracellular mouth of the pore regulate anion conduction in the CFTR chloride channel. *J. Gen. Physiol.* **2006**, *128*, 535–545.
- (51) Schultz, B. D.; Singh, A. K.; Devor, D. C.; Bridges, R. J. Pharmacology of CFTR chloride channel activity. *Physiol. Rev.* **1999**, *79*, S109–S144.
- (52) Wang, W.; El Hiani, Y.; Linsdell, P. Alignment of transmembrane regions in the cystic fibrosis transmembrane conductance regulator chloride channel pore. *J. Gen. Physiol.* **2011**, *138*, 165–178.
- (53) Liu, X.; Dawson, D. C. CFTR: Temperature-dependent cysteine reactivity suggests different stable conformers of the conduction pathway. *Biochemistry* **2011**, *50*, 10311–10317.
- (54) Krogh, A.; Larsson, B.; von Heijne, G.; Sonnhammer, E. L. Predicting transmembrane protein topology with a hidden Markov model: application to complete genomes. *J. Mol. Biol.* **2001**, *305*, 567–580.
- (55) Tusnady, G. E.; Simon, I. The HMMTOP transmembrane topology prediction server. *Bioinformatics* **2001**, *17*, 849–850.

- (56) Juretic, D.; Zoranic, L.; Zucic, D. Basic charge clusters and predictions of membrane protein topology. *J. Chem. Inf. Comput. Sci.* **2002**, *42*, 620–632.
- (57) Bryson, K.; McGuffin, L. J.; Marsden, R. L.; Ward, J. J.; Sodhi, J. S.; Jones, D. T. Protein structure prediction servers at University College London. *Nucleic Acids Res.* **2005**, *33*, W36–W38.
- (58) Petrey, D.; Xiang, Z.; Tang, C. L.; Xie, L.; Gimpelev, M.; Mitros, T.; Soto, C. S.; Goldsmith-Fischman, S.; Kernysky, A.; Schlessinger, A.; Koh, I. Y.; Alexov, E.; Honig, B. Using multiple structure alignments, fast model building, and energetic analysis in fold recognition and homology modeling. *Proteins* **2003**, *53*, 430–435.
- (59) Soding, J.; Biegert, A.; Lupas, A. N. The HHpred interactive server for protein homology detection and structure prediction. *Nucleic Acids Res.* **2005**, *33*, W244–W248.
- (60) Jaroszewski, L.; Rychlewski, L.; Li, Z.; Li, W.; Godzik, A. FFAS03: a server for profile–profile sequence alignments. *Nucleic Acids Res.* **2005**, *33*, W284–W288.
- (61) Jordan, I. K.; Kota, K. C.; Cui, G.; Thompson, C. H.; McCarty, N. A. Evolutionary and functional divergence between the cystic fibrosis transmembrane conductance regulator and related ATP-binding cassette transporters. *Proc. Natl. Acad. Sci. U.S.A.* **2008**, *105*, 18865–18870.
- (62) Hubbard, T.; Andrews, D.; Caccamo, M.; Cameron, G.; Chen, Y.; Clamp, M.; Clarke, L.; Coates, G.; Cox, T.; Cunningham, F.; Curwen, V.; Cutts, T.; Down, T.; Durbin, R.; Fernandez-Suarez, X. M.; Gilbert, J.; Hammond, M.; Herrero, J.; Hotz, H.; Howe, K.; Iyer, V.; Jekosch, K.; Kahari, A.; Kasprzyk, A.; Keefe, D.; Keenan, S.; Kokocinski, F.; London, D.; Longden, I.; McVicker, G.; Melsopp, C.; Meidl, P.; Potter, S.; Proctor, G.; Rae, M.; Rios, D.; Schuster, M.; Searle, S.; Severin, J.; Slater, G.; Smedley, D.; Smith, J.; Spooner, W.; Stabenau, A.; Stalker, J.; Storey, R.; Trevanion, S.; Ureta-Vidal, A.; Vogel, J.; White, S.; Woodwark, C.; Birney, E. ENSEMBL 2005. *Nucleic Acids Res.* **2005**, *33*, D447–D453.
- (63) Katoh, K.; Kuma, K.; Toh, H.; Miyata, T. MAFFT version 5: improvement in accuracy of multiple sequence alignment. *Nucleic Acids Res.* **2005**, *33*, 511–518.
- (64) Guindon, S.; Gascuel, O. A simple, fast, and accurate algorithm to estimate large phylogenies by maximum likelihood. *Syst. Biol.* **2003**, *52*, 696–704.
- (65) Landau, M.; Mayrose, I.; Rosenberg, Y.; Glaser, F.; Martz, E.; Pupko, T.; Ben-Tal, N. ConSurf 2005: the projection of evolutionary conservation scores of residues on protein structures. *Nucleic Acids Res.* **2005**, *33*, W299–W302.
- (66) Stevens, T. J.; Arkin, I. T. Substitution rates in alpha-helical transmembrane proteins. *Protein Sci.* **2001**, *10*, 2507–2517.
- (67) Fleishman, S. J.; Ben-Tal, N. Progress in structure prediction of alpha-helical membrane proteins. *Curr. Opin. Struct. Biol.* **2006**, *16*, 496–504.
- (68) Donnelly, D.; Overington, J. P.; Ruffe, S. V.; Nugent, J. H.; Blundell, T. L. Modeling alpha-helical transmembrane domains: the calculation and use of substitution tables for lipid-facing residues. *Protein Sci.* **1993**, *2*, 55–70.
- (69) Adamian, L.; Liang, J. Prediction of transmembrane helix orientation in polytopic membrane proteins. *BMC Struct. Biol.* **2006**, *6*, 13.
- (70) Sali, A.; Blundell, T. L. Comparative protein modelling by satisfaction of spatial restraints. *J. Mol. Biol.* **1993**, *234*, 779–815.
- (71) Wang, Y.; Loo, T. W.; Bartlett, M. C.; Clarke, D. M. Correctors promote maturation of CFTR processing mutants by binding to the protein. *J. Biol. Chem.* **2007**, *282*, 33247–33251.
- (72) Chen, E. Y.; Bartlett, M. C.; Loo, T. W.; Clarke, D. M. The DeltaF508 mutation disrupts packing of the transmembrane segments of the cystic fibrosis transmembrane conductance regulator. *J. Biol. Chem.* **2004**, *279*, 39620–39627.
- (73) Zhou, J. J.; Li, M. S.; Qi, J.; Linsdell, P. Regulation of conductance by the number of fixed positive charges in the intracellular vestibule of the CFTR chloride channel pore. *J. Gen. Physiol.* **2010**, *135*, 229–245.
- (74) Lomize, M. A.; Lomize, A. L.; Pogozheva, I. D.; Mosberg, H. I. OPM: Orientations of Proteins in Membranes database. *Bioinformatics* **2006**, *22*, 623–625.
- (75) Phillips, J. C.; Braun, R.; Wang, W.; Gumbart, J.; Tajkhorshid, E.; Villa, E.; Chipot, C.; Skeel, R. D.; Kale, L.; Schulten, K. Scalable molecular dynamics with NAMD. *J. Comput. Chem.* **2005**, *26*, 1781–1802.
- (76) Brooks, B. R.; Bruccoleri, R. E.; Olafson, B. D.; States, D. J.; Swaminathan, S.; Karplus, M. CHARMM: A Program for Macromolecular Energy, Minimization, and Dynamics Calculations. *J. Comput. Chem.* **1983**, *4*, 187–217.
- (77) GNUPLOT, version 4.4.3; 2011; <http://www.gnuplot.info>.